Journal of Computational Physics 469 (2022) 111535

Contents lists available at ScienceDirect

Journal of Computational Physics

www.elsevier.com/locate/jcp

Dynamic local coupling for multiphase flow: A compromise between efficiency and stability

Hanyu Li *, Mary F. Wheeler

Oden Institute for Computational Engineering and Sciences, United States of America

ARTICLE INFO

Article history:
Received 7 November 2021
Received in revised form 3 August 2022
Accepted 9 August 2022
Available online 17 August 2022

Keywords:
Local coupling
Convergence stability
Operator splitting
Error estimate
Smoothing

ABSTRACT

Complex models involving numerous coupled physical processes create substantial computational challenge. This paper introduces a solver algorithm that maintains a locally fully coupled system in the subdomains in which individual physical process interacts with other processes strongly. Meanwhile, the solutions in the other regions are treated in a decoupled fashion. The fully coupled regions are updated dynamically by either different timesteps or iterations. Global coupling of multiple physics generally results in systems with large number of unknowns that are computationally unfeasible. On the other hand, decoupling strategies alleviates the computational load, but results in stability issues, especially for nonlinear problems and sometimes encounters divergence during the solution process. The local coupling strategy applies error estimators to determine the strength of interaction between the physical processes in subdomains. By maintaining the system in fully coupled form within critical regions, the stability issue from the decoupling strategies is avoided while the computational load is significantly reduced as compared to a global coupling strategy.

1. Introduction

Complex model problems such as fluid-structure interaction and multiphase reactive transport involve numerous coupled physical processes. Attempting to approach the solution of these models in a monolithic fashion generates enormous linear systems that are computationally demanding even in parallel computing environments. To reduce the computational load, many algorithms aim to decouple the physics and solve the processes sequentially and iteratively until some convergence criterion is satisfied. Such strategy reduces the linear system size of each iteration significantly and thus improves computational efficiency.

Many decoupling algorithms regarding different model problems have been proposed. To mention a few works, for coupled flow and geomechanics problem, [10,11] investigated the accuracy and stability of different strategies of splitting the full Biot system. Lu and Wheeler [19] further improves current geomechanics decoupling schemes by avoiding unnecessary updates on the mechanic system during iterations. Wong et al. [26] applied sequential Newton method to transport problem with thermodynamics effects and [1] proposed a sequential solution algorithm for reactive transport. Although improving computational efficiency, the decoupled schemes naturally possess stability issues. For coupled flow and geomechanics problem, only fixed stress and undrained splitting algorithms have rigorous proof provided by [20] to be a contraction mapping

* Corresponding author.
E-mail addresses: lihanyu234@utexas.edu (H. Li), mfw@oden.utexas.edu (M.F. Wheeler).

https://doi.org/10.1016/j.jcp.2022.111535
0021-9991/

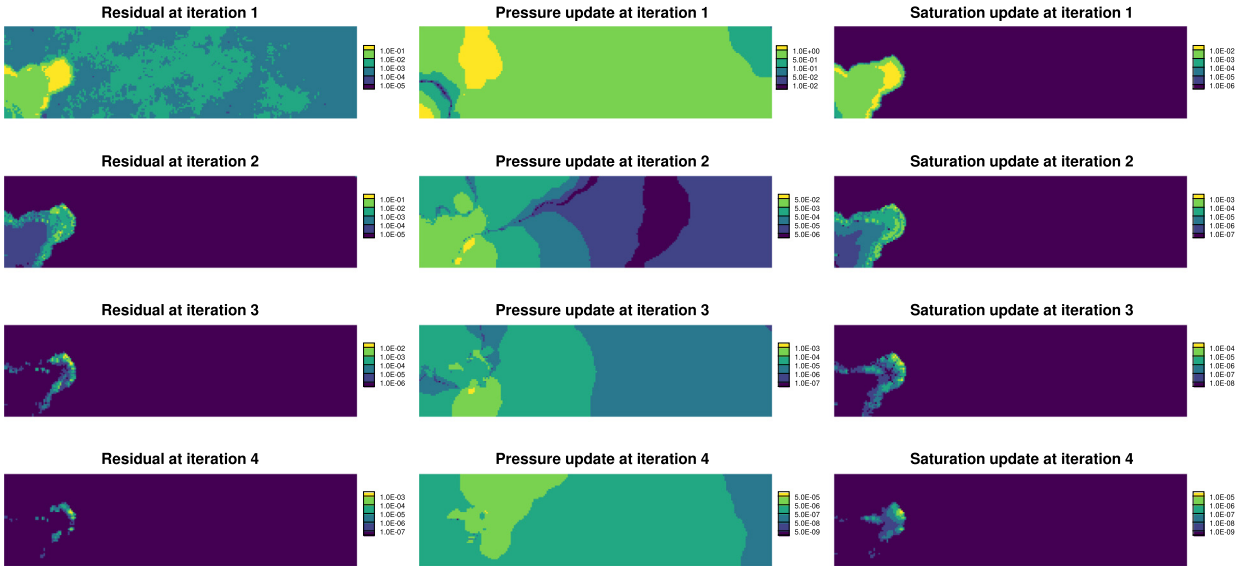

Fig. 1. Pressure and saturation updates during Newton iterations for a typical timestep. (For interpretation of the colors in the figure(s), the reader is referred to the web version of this article.)

and thus admits a unique solution. Although each sequential iteration requires a lot less computation to resolve, decoupling thermodynamics and reactive transport problems results in a lot more iterations to achieve convergence.

Regarding multiphase flow problems, implicit pressure explicit saturation (IMPES) method is successful in two phase slightly-compressible fluid models, since the total mobility ratio stays fairly constant as saturation changes and therefore the advection decouples naturally from the diffusion process. As fluid behavior becomes more complicated, such method starts to show stability and divergence issues. To mitigate the problem, the adaptive implicit formulation was proposed [5,7,22,27] such that only the subdomains with significant variation in saturation/concentration are solved fully implicitly. Although resolving the stability issue, such algorithms do not provide significant computational speedup. To be more specific, since the regions with less variation are embedded explicitly, the adaptive implicit and fully implicit formulation have the same system size. Meanwhile, such embedding destroys the banded and symmetric structure of the Jacobian matrix which makes the performance of iterative solvers such as GMRES suboptimal. The explicit part of the system also imposes a limit on the timestep size for stable Newtonian convergence.

The transport process in the multiphase flow model is mainly governed by the Buckley-Leverett equation as follows

$$\frac{\partial S}{\partial t} + \nabla \cdot (f(S)\boldsymbol{u}) = 0, \tag{1.1}$$

which is a first order hyperbolic system. Unlike the parabolic diffusion process which occurs on a global scale, the hyperbolic transport exists locally. Fig. 1 illustrates the pressure and saturation updates of a two-phase flow model during Newton iterations of a typical timestep. We observe the pressure updates throughout the entire domain while the saturation updates are mainly concentrated at the saturation front. Keeping the saturation front regions in a fully coupled formulation while decoupling the saturation unknowns in other domains can reduce the computational load without adding convergence bottlenecks.

In this paper, we introduce a dynamic local coupling method for solving multiphase flow problems. In Section 2 we present the model problem followed by a local coupling algorithm in Section 4. Results from both slightly-compressible and fully compressible fluid are presented in Section 5. We will then discuss the application of such algorithm to a space-time geometric multigrid method in Section 6. Conclusions follow in Section 7.

2. Flow model problem

We consider the following two-phase flow in porous media model. The phase mass conservation, constitutive equations, boundary and initial conditions are as follows:

$$\frac{\partial(\phi \rho_\alpha s_\alpha)}{\partial t} + \nabla \cdot \boldsymbol{u}_\alpha = q_\alpha \quad in\ \Omega \times J, \tag{2.1}$$

$$\boldsymbol{u}_\alpha = -K \rho_\alpha \frac{k_{r\alpha}}{\mu_\alpha} (\nabla p_\alpha - \rho_\alpha \boldsymbol{g}) \quad in\ \Omega \times J, \tag{2.2}$$

$$\boldsymbol{u}_\alpha \cdot \boldsymbol{\nu} = 0 \quad on\ \partial\Omega \times J, \tag{2.3}$$

$$\begin{cases} p_\alpha = p_\alpha^0 \\ s_\alpha = s_\alpha^0 \end{cases} \quad at\ \Omega \times \{t = 0\}. \tag{2.4}$$

Here, ϕ is porosity and K is permeability tensor. ρ_α, s_α, $\boldsymbol{u}_\alpha$ and q_α are density, saturation, velocity and source/sink, respectively for each phase. The phase densities are calculated by Eqn. (2.5) and (2.6) depending on whether they are slightly or fully compressible

$$\rho_\alpha = \rho_{\alpha,ref} \cdot e^{c_\alpha (p_\alpha - p_{\alpha,ref})}, \tag{2.5}$$

$$\rho_\alpha = \rho_{\alpha,ref} \cdot c_\alpha p_\alpha. \tag{2.6}$$

c_α is the fluid compressibility and $\rho_{\alpha,ref}$ is the reference density at reference pressure $p_{\alpha,ref}$. In addition, $k_{r\alpha}$, μ_α and p_α are the relative permeability, viscosity and pressure for each phase. The relative permeability is a function of saturation. Pressure differs between wetting phase and non-wetting phase in the presence of capillary pressure, which is also a function of saturation:

$$k_{r\alpha} = f(s_\alpha), \tag{2.7}$$

$$p_c = g(s_\alpha) = p_{nw} - p_w. \tag{2.8}$$

The saturation of all phases obeys the following constraint:

$$\sum_\alpha s_\alpha = 1. \tag{2.9}$$

We use mixed finite element method to resolve the system. The functional spaces for pressure/saturation and velocity are

$$\boldsymbol{V} = H(div; \Omega) = \left\{ \boldsymbol{v} \in \left(L^2(\Omega)\right)^d : \nabla \cdot \boldsymbol{v} \in L^2(\Omega) \right\}, \quad W = L^2(\Omega),$$

with finite dimensional subspaces as $\boldsymbol{V}_h$ and W_h. Let $J = (0, T]$ be partitioned in to a number of coarse time intervals $\{t_n\}_{n=1}^N$ where $0 = t_1 < t_2 < \cdots < t_N = T$. $J_n = (t_n, t_{n+1}]$ is the nth partition of the time domain of interest. Then the mixed method weak formulation of Eqn. (2.1) and (2.2) are: find $\boldsymbol{u}_{\alpha,h}^n \in \boldsymbol{V}_h$, $\tilde{\boldsymbol{u}}_{\alpha,h}^n \in \boldsymbol{V}_h$, $s_{\alpha,h}^n \in W_h$, $p_{\alpha,h}^n \in W_h$ such that

$$\int_{J_n}\int_\Omega \partial_t \left(\phi \rho_{\alpha,h}^n s_{\alpha,h}^n\right) w + \int_{J_n}\int_\Omega \left(\nabla \cdot \boldsymbol{u}_{up,\alpha,h}^n\right) w = \int_{J_n}\int_\Omega q_\alpha w \quad \forall w \in W_h, \tag{2.10}$$

$$\int_{J_n}\int_\Omega K^{-1} \tilde{\boldsymbol{u}}_{\alpha,h}^n \cdot \boldsymbol{v} = \int_{J_n}\int_\Omega p_{\alpha,h}^n \nabla \cdot \boldsymbol{v} \quad \forall \boldsymbol{v} \in \boldsymbol{V}_h, \tag{2.11}$$

$$\int_{J_n}\int_\Omega \boldsymbol{u}_{\alpha,h}^n \cdot \boldsymbol{v} = \int_{J_n}\int_\Omega \lambda_\alpha \tilde{\boldsymbol{u}}_{\alpha,h}^n \cdot \boldsymbol{v} \quad \forall \boldsymbol{v} \in \boldsymbol{V}_h. \tag{2.12}$$

The mobility ratio in λ_α is defined as

$$\lambda_\alpha = \frac{k_{r\alpha}\rho_\alpha}{\mu_\alpha}, \tag{2.13}$$

and the upwind velocity is calculated by

$$\int_{J_n}\int_\Omega \boldsymbol{u}_{up,\alpha,h}^n \cdot \boldsymbol{v} = \int_{J_n}\int_\Omega \lambda_\alpha^* \tilde{\boldsymbol{u}}_{\alpha,h}^n \cdot \boldsymbol{v} \quad \forall \boldsymbol{v} \in \boldsymbol{V}_h. \tag{2.14}$$

The additional auxiliary phase fluxes $\tilde{\boldsymbol{u}}_{\alpha,h}^n$ is used to avoid inverting zero phase relative permeability [21]. Calculation of the upwind mobility ratio is done by using saturations from the grid cell on the upwind direction of the pressure gradient.

3. Coupling strength

In multiphase flow problems, the subdomains with strong transport-diffusion coupling are characterized by a dramatic saturation change in time. In such regions, the fluid flow is not dominated by a single phase and therefore the solution is strongly dependent upon both pressure and saturation. It is also the main source of nonlinearity that requires multiple Newton iterations for convergence, while the remaining regions behave near linearly. Here, we use temporal error estimators

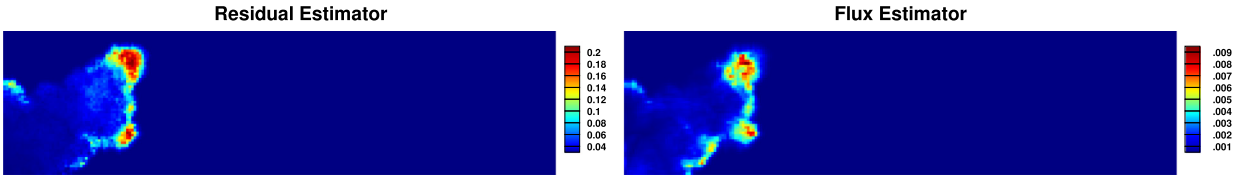

Fig. 2. Temporal residual and flux error estimators for determining coupling regions.

$\eta^n_{E,t,r,\alpha}$ and $\eta^n_{E,t,f,\alpha}$ introduced in [14], which characterize the discretization error in time, to determine the subdomains with strong coupling:

$$\eta^n_{E,t,r,\alpha} = |T_i|\left(\int_{E_i} \left|\partial_t\left(\phi\rho^n_{\alpha,h}s^n_{\alpha,h}\right) + \nabla\cdot\boldsymbol{u}^n_{up,\alpha,h} - q_\alpha\right|^2\right)^{\frac{1}{2}}, \tag{3.1}$$

$$\eta^n_{E,t,f,\alpha} = \left(\int_{E_i} K^{-1}\left|\boldsymbol{u}^n_{\alpha,h} - \boldsymbol{u}^n_{\alpha,h\tau}\right|^2\right)^{\frac{1}{2}}. \tag{3.2}$$

These are element-wise estimators for each $E_i = T_i \times F_i$ in partition $\mathcal{T}^n_h$ of $\Omega \times J_n$. Similar error estimators are also derived in [23,24]. The subscript τ indicates the affine globally continuous function in each interval J_n for $1 \le n \le N$ defined as

$$f^n_\tau = f^{n-1} + \frac{t - t_{n-1}}{\Delta t}(f^n - f^{n-1}) \quad t \in J_n, \tag{3.3}$$

for any discrete function in time f^n. As illustrated in Fig. 2, the error estimators outline the critical regions that require fully coupled formulation for stable numerical solution.

We now show that the two error indicators mentioned above provide a measure of coupling strength between the advection and the diffusion. Let us define the phase residual at each Newton iteration as

$$R^{n,l}_{\alpha,h} = \int_{J_n}\int_{\Omega} \left(\partial_t(\phi\rho^{n,l}_{\alpha,h}s^{n,l}_{\alpha,h}) + \nabla\cdot\boldsymbol{u}^{n,l}_{\alpha,h} - q_\alpha\right)w, \tag{3.4}$$

with its absolute value measuring the proximity of the current state $\{p^{n,l}_{\alpha,h}, s^{n,l}_{\alpha,h}, \boldsymbol{u}^{n,l}_{\alpha,h}\}$ to the converged solution $\{p^n_{\alpha,h}, s^n_{\alpha,h}, \boldsymbol{u}^n_{\alpha,h}\}$. We assume the iterations approaches convergence monotonically such that the residual at each iteration has the same sign. Let k denote the number of iterations required for Newton's method to converge and assume the iterations produce a set of increments $\{\delta p^{n,l}_{\alpha,h}, \delta s^{n,l}_{\alpha,h}, \delta\boldsymbol{u}^{n,l}_{\alpha,h}\}_{l=1}^k$. We now define $\{\delta t^{n,l}\}$ be a set of artificial incremental time defined such that

$$\delta t^{n,l}\partial_t\boldsymbol{u}^n_{\alpha,h\tau} = \delta\boldsymbol{u}^{n,l}_{\alpha,h}. \tag{3.5}$$

Since $\sum_{l=1}^k \delta\boldsymbol{u}^{n,l}_{\alpha,h} = \boldsymbol{u}^n_{\alpha,h} - \boldsymbol{u}^{n-1}_{\alpha,h}$, then

$$\boldsymbol{u}^n_{\alpha,h} - \boldsymbol{u}^{n-1}_{\alpha,h} = \sum_{l=1}^k \delta t^{n,l}\partial_t\boldsymbol{u}_{\alpha,h\tau} = \frac{\boldsymbol{u}^n_{\alpha,h} - \boldsymbol{u}^{n-1}_{\alpha,h}}{\Delta t}\sum_{l=1}^k \delta t^{n,l} \quad \Rightarrow \quad \sum_{l=1}^k \delta t^{n,l} = \Delta t = |J_n|.$$

It stems from Eq. (3.4) that the "distance" traveled during each iteration is defined as

$$r^{n,l}_{\alpha,h} = \frac{\delta t^{n,l}}{2|J_n|}\left(R^{n,l}_{\alpha,h} + R^{n,l-1}_{\alpha,h}\right) = \frac{\delta t^{n,l}}{2|J_n|}\int_{J_n}\int_{\Omega} \left(\partial_t(\phi\rho^{n,l}_{\alpha,h}s^{n,l}_{\alpha,h}) + \partial_t(\phi\rho^{n,l-1}_{\alpha,h}s^{n,l-1}_{\alpha,h}) + \nabla\cdot\boldsymbol{u}^{n,l}_{\alpha,h} + \nabla\cdot\boldsymbol{u}^{n,l-1}_{\alpha,h} - 2q_\alpha\right)w. \tag{3.6}$$

We also have

$$\int_{J_n}\int_{\Omega} \left(\partial_t(\phi\rho^n_{\alpha,h}s^n_{\alpha,h}) + \nabla\cdot\boldsymbol{u}^n_{\alpha,h} - q_\alpha\right)w = 0. \tag{3.7}$$

Then we have the total "distance" traveled during the iteration process as

$$\begin{aligned}\left|\sum_{l=1}^k r^{n,l}_{\alpha,h}\right| &= \left|\sum_{l=1}^k \frac{\delta t^{n,l}}{2}\int_{\Omega} \left(\phi\frac{\rho^{n,l}_{\alpha,h}s^{n,l}_{\alpha,h} + \rho^{n,l-1}_{\alpha,h}s^{n,l-1}_{\alpha,h} - 2\rho^n_{\alpha,h}s^n_{\alpha,h}}{|J_n|} + \nabla\cdot\boldsymbol{u}^{n,l}_{\alpha,h} + \nabla\cdot\boldsymbol{u}^{n,l-1}_{\alpha,h} - 2\nabla\cdot\boldsymbol{u}^n_{\alpha,h}\right)w\right| \\ &\le I_1 + I_2.\end{aligned} \tag{3.8}$$

By trapezoidal rule, we take the following

$$\begin{aligned} I_1 &= \left| \sum_{l=1}^{k} \frac{\delta t^{n,l}}{2} \int_{\Omega} \left(\nabla \cdot \boldsymbol{u}_{\alpha,h}^{n,l} + \nabla \cdot \boldsymbol{u}_{\alpha,h}^{n,l-1} - 2\nabla \cdot u_{\alpha,h}^{n} \right) w \right| \\ &= \left| \sum_{l=1}^{k} \frac{\delta t^{n,l}}{2} \int_{\Omega} \left(\nabla \cdot \boldsymbol{u}_{\alpha,h}^{n,l} + \nabla \cdot \boldsymbol{u}_{\alpha,h}^{n,l-1} \right) w - \int_{J_n} \int_{\Omega} \nabla \cdot \boldsymbol{u}_{\alpha,h}^{n} w \right| \\ &= \left| \int_{J_n} \int_{\Omega} \nabla \cdot \left(\boldsymbol{u}_{\alpha,h\tau}^{n} - \boldsymbol{u}_{\alpha,h}^{n} \right) w \right|. \end{aligned} \tag{3.9}$$

With the relation

$$\int_{E} \nabla \cdot \left(\boldsymbol{u}_{\alpha,h\tau}^{n} - \boldsymbol{u}_{\alpha,h}^{n} \right) = \int_{\partial E} \left(\boldsymbol{u}_{\alpha,h\tau}^{n} - \boldsymbol{u}_{\alpha,h}^{n} \right) \cdot \boldsymbol{n}, \tag{3.10}$$

we obtain

$$\begin{aligned} I_1 &= \left| \sum_{E \in \mathcal{T}_h^n} \int_{E} \nabla \cdot \left(\boldsymbol{u}_{\alpha,h\tau}^{n} - \boldsymbol{u}_{\alpha,h}^{n} \right) w \right| \leq \sum_{E \in \mathcal{T}_h^n} \int_{\partial E} \left| w \left(\boldsymbol{u}_{\alpha,h\tau}^{n} - \boldsymbol{u}_{\alpha,h}^{n} \right) \cdot \boldsymbol{n} \right| \leq \sum_{E \in \mathcal{T}_h^n} \int_{E} \left| \left(\boldsymbol{u}_{\alpha,h\tau}^{n} - \boldsymbol{u}_{\alpha,h}^{n} \right) w \right| \\ &\leq C \| w \|_{L^2(\Omega)} \Big(\sum_{E \in \mathcal{T}_h^n} (\eta_{E,t,f,\alpha}^{n})^2 \Big)^{\frac{1}{2}}. \end{aligned} \tag{3.11}$$

For the remaining part, we also have

$$\begin{aligned} I_2 &= \left| \sum_{l=1}^{k} \frac{\delta t^{n,l}}{2} \int_{\Omega} \phi \frac{\rho_{\alpha,h}^{n,l} s_{\alpha,h}^{n,l} + \rho_{\alpha,h}^{n,l-1} s_{\alpha,h}^{n,l-1}}{|J_n|} w - \int_{\Omega} \phi \rho_{\alpha,h}^{n} s_{\alpha,h}^{n} w \right| \\ &\leq \left| \int_{\Omega} \phi (\rho_{\alpha,h}^{n} s_{\alpha,h}^{n} - \rho_{\alpha,h}^{n-1} s_{\alpha,h}^{n-1}) w \right| \\ &\leq C \| w \|_{L^2(\Omega)} \Big(\sum_{E \in \mathcal{T}_h^n} \int_{E} \left| \phi (\rho_{\alpha,h}^{n} s_{\alpha,h}^{n} - \rho_{\alpha,h}^{n-1} s_{\alpha,h}^{n-1}) \right|^2 \Big)^{\frac{1}{2}}. \end{aligned} \tag{3.12}$$

As demonstrated, the coupling strength includes contributions from both nonlinear phase advection and phase accumulation. Since accumulation changes mostly coincide with the variations in phase flux, therefore determining the coupling strength with the flux error indicator is sufficient. Meanwhile, due to the close resemblance between $\eta_{E,t,r,\alpha}$ and $R_{\alpha,h}^{n,l}$, the residual error indicator naturally provides a rough estimate for the coupling strength at each iteration, by measuring the "distance" between the current state and the converged solution. However, the coupling strength computed in such a fashion requires to be updated at each Newton iteration.

4. Dynamic local coupling algorithm

Unlike the two methods, namely the adaptive implicit method that treats certain domains explicitly and the IMPES method that solves pressure and saturation in separate systems, the dynamic local coupling method first determines the subdomains where transport is strongly coupled with diffusion. Then, the saturation unknowns in strong coupling regions are merged with the global pressure unknowns to be solved monolithically. An example of such a strategy is illustrated in Fig. 3. On the left is a sample 2D grid with red index indicating strong transport-diffusion coupling. The corresponding Jacobian matrix is presented on the right. Unlike the fully implicit monolithic system, such matrix is not banded but is still symmetric.

We propose two dynamic local coupling algorithms to separate the difference in convergence behavior. The first type is a timestep dynamic. We evaluate the error estimators of the fluid phases at the beginning of each timestep to determine the locally coupled system and a remainder system that consists of all saturation unknowns that are decoupled. Then the two systems are solved iteratively and implicitly until convergence. During the iterations of a given timestep, the structure of the two systems are fixed. The algorithm is described in Algorithm 1. Unlike the IMPES approach or sequential method for compositional simulation [17], we do not require internal loops for either systems to converge to a required tolerance before continuing to the other. An example of the coupling subdomain map for early and late simulation time is illustrated in Fig. 4.

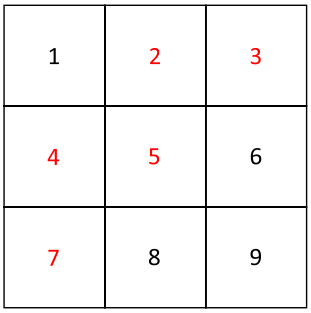

	p_1	p_2	s_2	p_3	s_3	p_4	s_4	p_5	s_5	p_6	p_7	s_7	p_8	p_9
$R_{1,p}$	x	x	x			x	x							
$R_{2,p}$	x	x	x	x	x			x	x					
$R_{2,s}$	x	x	x	x	x			x	x					
$R_{3,p}$		x	x	x	x					x				
$R_{3,s}$		x	x	x	x					x				
$R_{4,p}$	x					x	x	x	x		x	x		
$R_{4,s}$	x					x	x	x	x		x	x		
$R_{5,p}$		x	x			x	x	x	x	x			x	
$R_{5,s}$		x	x			x	x	x	x	x			x	
$R_{6,p}$				x	x			x	x	x				x
$R_{7,p}$						x	x				x	x	x	
$R_{7,s}$						x	x				x	x	x	
$R_{8,p}$								x	x		x	x	x	x
$R_{9,s}$										x			x	x

Fig. 3. Sample grid (red index cells use fully coupled formulation) and the structure of the corresponding Jacobian matrix.

Algorithm 1 Timestep dynamic local coupling.

while $t_n \leq T$ **do**
  Calculate $\eta^n_{E,t,r,\alpha}$
  if $\eta^n_{E,t,r,\alpha} > \eta^n_{t,r,thresh}$ or $\eta^n_{E,t,f,\alpha} > \eta^n_{t,f,thresh}$ **then**
    Set E_i in local coupling map
  end if
  ▷ threshold values are the logarithmic mode of the data
  while $\|R^{n,k}\|_\infty > \varepsilon_{Newton}$ **do**
    Solve locally coupled system
    Solve remainder system
    Calculate $R^{n,k+1}$ and check convergence
    $k \leftarrow k+1$
  end while
  Calculate $\eta^n_{E,t,f,\alpha}$
  $n \leftarrow n+1$
  $\eta^n_{E,t,f,\alpha} \leftarrow \eta^{n-1}_{E,t,f,\alpha}$
end while

Fig. 4. Local coupling subdomain determined for left: a early timestep and right: a late time timestep.

The second type is iteration dynamic. Before each Newton iteration, error estimators are reevaluated to update the local coupling map while the first iteration of any timestep couples the entire domain. During the reevaluation, subdomains that already satisfies a convergence criterion for the advection process are excluded from the map. Consequently once excluded, saturation unknowns in the decoupled region are no longer updated for the remaining iterations of a timestep. The algorithm is described in Algorithm 2. An example of the coupling subdomain map for each iteration is illustrated in Fig. 5. The colored region rapidly converges to the saturation front which is only a small portion of the global system. To update the map for each iteration efficiently, only the coupled regions of the previous iteration are evaluated for the error estimators, instead of the global domain. For more efficient convergence behavior, a phase scaling [18] formulation is applied to all the decoupled regions.

5. Numerical results

We apply the SPE10 dataset [3] layer 52 to demonstrate our numerical algorithms. The petrophysical property is shown in Fig. 6. We choose a channelized distribution since such type illustrates more severe computational bottleneck. The global

Algorithm 2 Iteration dynamic local coupling.

while $t_n \leq T$ **do**
  Set local coupling domain to global
  while $\|R^{n,k}\|_\infty > \varepsilon_{Newton}$ **do**
    Solve locally coupled system
    Calculate $R^{n,k+1}$ and check convergence
    Calculate $\eta^{n,k+1}_{E,t,r,\alpha}$, $\eta^{n,k+1}_{E,t,f\alpha}$ in local coupling domain of iteration k
    if $\eta^{n,k+1}_{E,t,r,\alpha} > \varepsilon_{Newton}$ or $\eta^{n,k+1}_{E,t,f\alpha} > \eta^{n,k+1}_{t,f,thresh}$ **then**
      Keep E in local coupling map
    else
      Remove E from local coupling map
    end if
    $k \leftarrow k+1$
  end while
  $n \leftarrow n+1$
end while

Fig. 5. Local coupling subdomain determined for each Newton iteration (the first iteration with global coupling is not omitted).

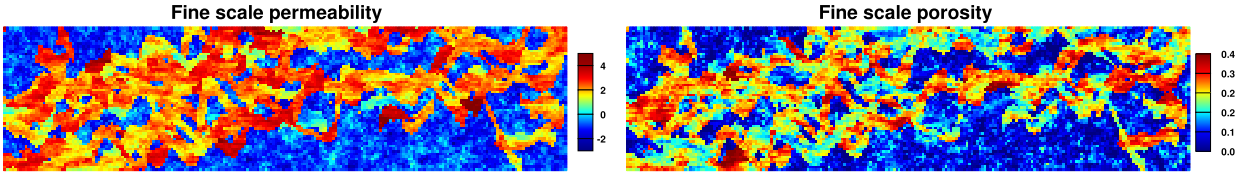

Fig. 6. Fine scale permeability (left) and porosity (right) for numerical experiment.

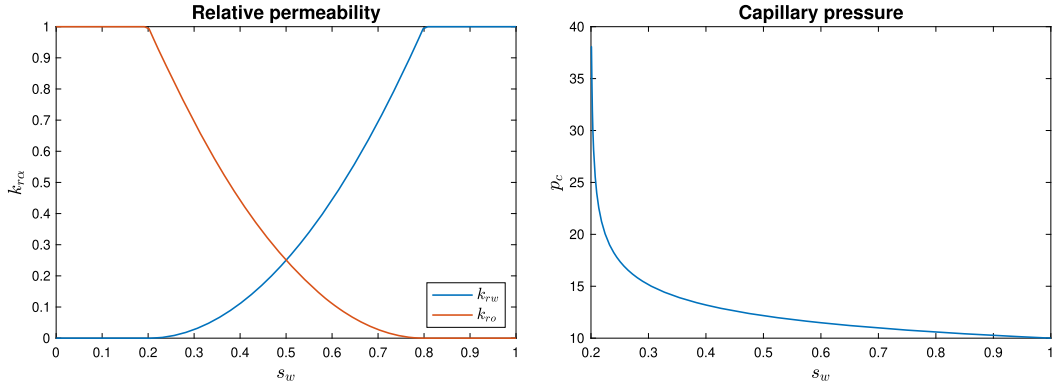

Fig. 7. Relative permeability (left) and capillary pressure (right) curve for numerical experiment.

domain has the dimension of 56×216 elements with the element size of $1ft \times 1ft \times 1ft$. For nonlinear transport, we use Brooks-Corey model plotted in Fig. 7 for both relative permeability and capillary pressure described by:

Table 1
Fluid data for numerical experiment.

Parameter	Value	Unit
Gas compressibility (c_g)	5.0×10^{-2}	psi^{-1}
Oil compressibility (c_o)	1.0×10^{-4}	psi^{-1}
Water compressibility (c_w)	3.0×10^{-6}	psi^{-1}
Gas viscosity (μ_g)	0.03	cp
Oil viscosity (μ_o)	3.0	cp
Water viscosity (μ_w)	1.0	cp
Gas standard density ($\rho_{g,std}$)	0.1	lb/ft^3
Oil standard density ($\rho_{o,std}$)	53	lb/ft^3
Water standard density ($\rho_{w,std}$)	64	lb/ft^3

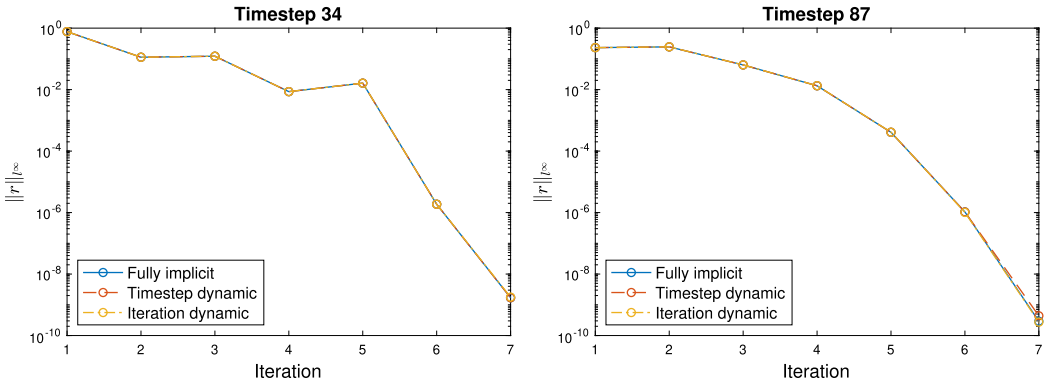

Fig. 8. Convergence behavior of difference methods at timesteps with strong nonlinearity for slightly compressible flow.

$$\begin{cases} k_{rw} = k_{rw}^0 \left(\dfrac{s_w - s_{wirr}}{1 - s_{or} - s_{wirr}} \right)^{n_w} \\ k_{ro} = k_{ro}^0 \left(\dfrac{s_o - s_{or}}{1 - s_{or} - s_{wirr}} \right)^{n_o} \end{cases}, \tag{5.1}$$

$$p_c(s_w) = P_{en,cow} \left(\frac{1 - s_{wirr}}{s_w - s_{wirr}} \right)^{l_{cow}}. \tag{5.2}$$

The model parameter values are $s_{or} = s_{wirr} = 0.2$, $k_{ro}^0 = k_{rw}^0 = 1.0$, $n_w = n_o = 2$, $p_{en,cow} = 10\ psi$ and $l_{cow} = 0.2$. For the fully compressible flow experiment, the gas phase takes the water phase relative permeability behavior. The capillary pressure relation stays the same, however with gas being the non-wetting phase. The fluid data are listed in Table 1.

5.1. Slightly compressible fluid

The oil-water system is used for slightly compressible numerical experiment. The initial pressure and water saturation are set at 1000 *psi* and 0.2 respectively. A rate specified water injection well is placed at the bottom left corner with an injection rate of 1 ft^3/day and a pressure specified production well is placed at the upper right corner with a production pressure of 1000 *psi*. The simulation stops at 500 days (water breakthrough) with the time step size of 1.25 days.

We first investigate the nonlinear convergence behavior of the different methods. Fig. 8 illustrates the maximum residual during Newton iterations for two sample timesteps with slow nonlinear convergence. Here we observe that both local coupling methods capture the same behavior as the fully implicit method. The residual reduction paths are almost identical. However, note that the residual in decoupled regions is calculated by phase scaling, and thus represents overall fluid mass balance instead of individual phases. Therefore, the decoupling schemes can be considered as indirectly loosening the convergence criterion.

With stepwise convergence behavior captured, the total iteration count, as demonstrated in Fig. 9, from iteration dynamic approach and fully implicit method are almost identical, while the count from timestep dynamic strategy is slightly higher. The iteration count for the timestep dynamic method is normalized by global domain, meaning that a solution for both locally coupled system and remainder system together counts as one full iteration. Regarding the computation time, the timestep dynamic approach provides about 50% speedup while the iteration dynamic method delivers 75%. The main reason for such difference is that the timestep dynamic method sweeps through the entire domain every Newton iteration while the iteration dynamic strategy reduces the system size gradually as it reaches final convergence. Also, the coupling region for timestep dynamic method during late simulation time is significantly larger, making the solution for the locally coupled

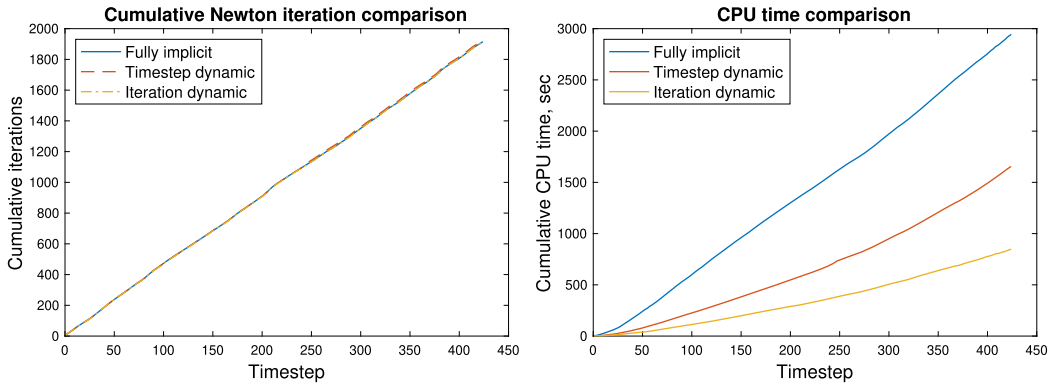

Fig. 9. Cumulative Newton iteration and CPU time comparison for slightly compressible fluid model.

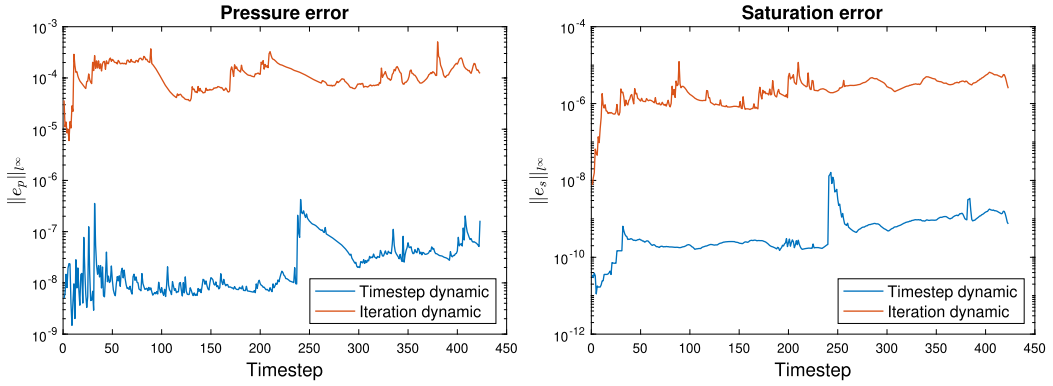

Fig. 10. Pressure and saturation error of timestep dynamic and iteration dynamic method for slightly compressible fluid model.

system more costly. Therefore we see the CPU time increases more sharply during late time for such algorithm while the increase stays fairly linear for the iteration dynamic method. However, a timestep dynamic algorithm is still a valuable approach for multi-physics models. For example for flow coupled with geomechanics, solving the monolithic system of a engineering scale model, even for just one iteration, is computationally infeasible. The timestep dynamic strategy can still provide considerable speedup while not adding severe stability issues that either increase the number of iterations to achieve convergence or cause divergence.

We confirm the accuracy of the local coupling methods by calculating the $\|\cdot\|_{l^\infty}$ of e_p and e_s, the difference in pressure and saturation against the fully implicit solution in the global domain. The results are presented in Fig. 10. The solution error from the iteration dynamic method is generally 4 orders of magnitude larger than the error from the timestep dynamic strategy. This is due to the iteration dynamic approach skipping the saturation update for the decoupled regions. Although not causing any macroscopic effects in the system, there still exists extremely small updates on saturation unknowns if the remainder system is solved, which will in return affect the pressure equation. Despite such deficiency, the errors are generally minimum. The largest pressure error is in the 10^{-4} range and the largest saturation error is in the 10^{-6} range. One could combine both methods for accuracy and scalable computational speedup during late time.

5.2. Fully compressible fluid

The gas-oil system is used for fully compressible numerical experiment. The initial pressure and gas saturation are set at 2500 psi and 0.2 respectively. A rate specified gas injection well is placed at the bottom left corner with an injection rate of 10 ft^3/day and a pressure specified production well is placed at the upper right corner with a production pressure of 2500 psi. The simulation stops at 300 days (gas breakthrough) with the time step size of 1.25 days.

The decoupled region maintains steady flowing state which results in minimum accumulation. However for fully compressible fluid, there may still be saturation change due to pressure fluctuations. Let $C_\alpha = \rho_\alpha s_\alpha = const$, then we have

$$dC_\alpha = d\rho_\alpha s_\alpha + \rho_\alpha ds_\alpha = s_\alpha \frac{d\rho_\alpha}{dp_\alpha} dp_\alpha + \rho_\alpha ds_\alpha = 0 \quad \Rightarrow \quad ds_\alpha = -\frac{s_\alpha}{\rho_\alpha}\frac{d\rho_\alpha}{dp_\alpha} dp_\alpha. \tag{5.3}$$

Such correction on saturation is essential for regions with no compressible phase flow when using iteration dynamic method, since the saturation is not explicitly updated after a subdomain is decoupled from the main system. The non-

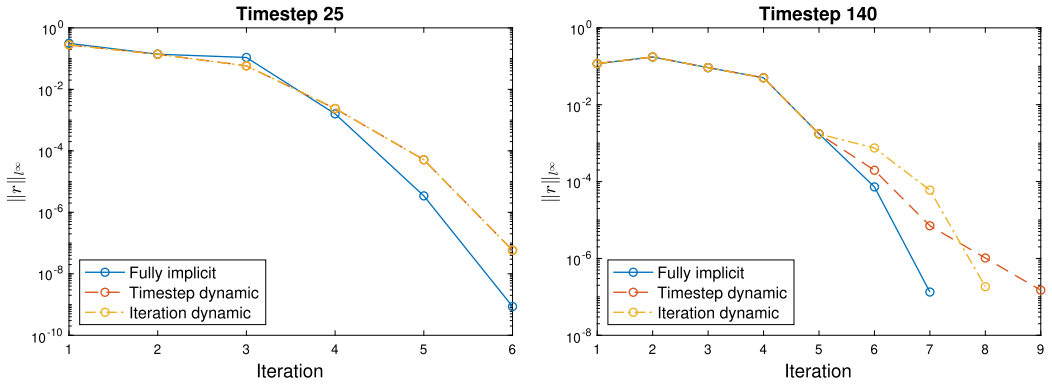

Fig. 11. Convergence behavior of difference methods at timesteps with strong nonlinearity for fully compressible flow.

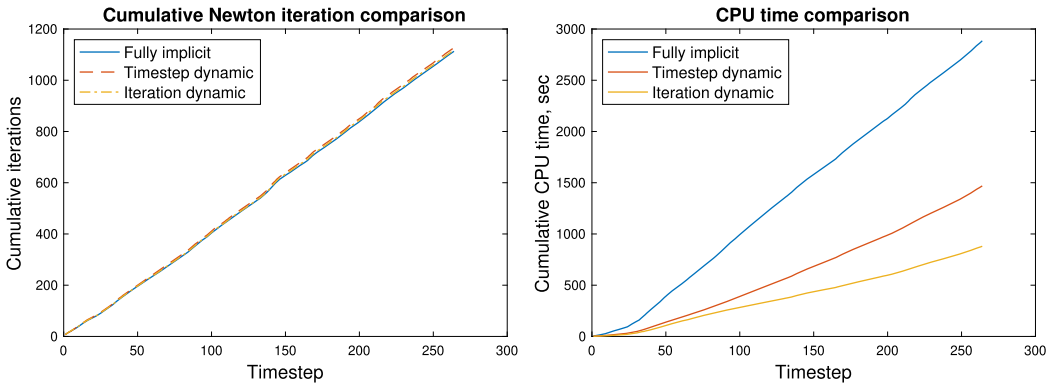

Fig. 12. Cumulative Newton iteration and CPU time comparison for fully compressible fluid model.

linear convergence behavior of two sample timesteps is illustrated in Fig. 11. Here we observe the decoupled methods follow the path of fully implicit method during early iterations but deviates toward final convergence. The number of iterations to achieve convergence may also vary for certain timesteps, even with corrections made by Eqn. (5.3). The error estimators utilized mainly quantify the nonlinearities caused by the transport process instead of diffusion. Consequently, regions with steady flow but large pressure disturbance are decoupled. Such pressure alteration can still cause noticeable effect on the saturation solution of the compressible phase and thus slows the convergence. Implementing additional error estimators that measures the nonlinearity caused by compressibility may alleviate such problem.

Despite the slower convergence at certain timesteps, the decoupling methods still provide considerable speedup for the compressible model. As demonstrated in Fig. 12, similar to the slightly compressible case, the cumulative Newton iteration count of the decoupling algorithms is still fairly close to the one from fully implicit approach. There's around 50% and 75% speedup using the timestep dynamic and the iteration dynamic approach respectively. Here we do not see a sharper increase in CPU time for the timestep dynamic method during late simulation time. Due to low viscosity, the gas phase behaves more diffusively. Consequently, the saturation solution behind the front stabilizes quickly and thus the local coupling domain size stays fairly constant during the simulation.

Again, we confirm the accuracy of the pressure and saturation solution. As illustrated in Fig. 13, due to strong compression effects tightening the connection between pressure and saturation, the error in this model is slightly higher than the slightly compressible case. The error from the timestep dynamic method remains low, approximately the 10^{-6} mark, and stable throughout the simulation. On the other hand, the error from the iteration dynamic approach is approximately 2 orders of magnitude larger and increases slightly over time. For the later method, the saturation in the decoupled subdomain is updated by the approximation using Eqn. (5.3) instead of solving a linear system, causing increased error in the solution. The strong compressibility also creates errors into the pressure solution. These errors propagate and expand as simulation continues and thus increase over time. Such behavior also indicates that combining the two decoupling strategies is beneficial for both accuracy and computational efficiency. Feedbacks from preliminary experiment combining the two methods suggests that a more detailed algorithm to update the local coupling regions is needed. Small "islands" in the decoupled region or "holes" in the coupling domain can hinder the nonlinear convergence significantly. An error estimator measuring the coupling strength [8] may be greatly beneficial.

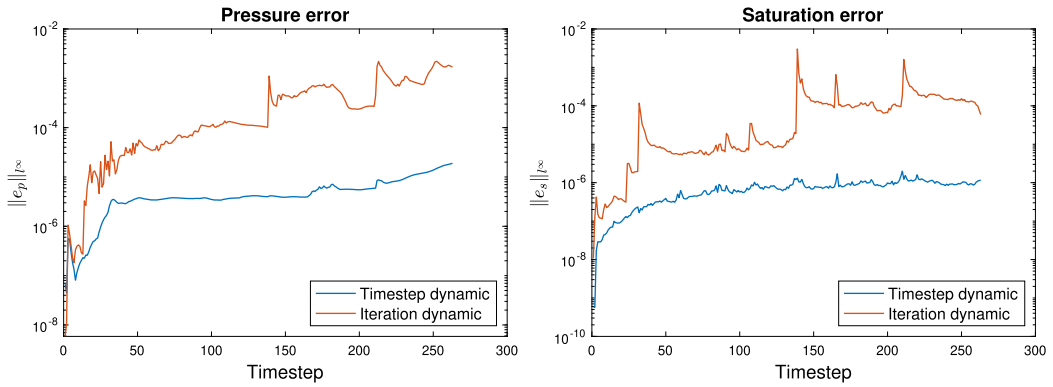

Fig. 13. Pressure and saturation error of timestep dynamic and iteration dynamic method for fully compressible fluid model.

6. Application to space-time algorithm

Space-time algorithms has shown promising results for improving computational efficiency of different problems [2,9,12,13]. The sequential refinement solver algorithm was introduced in [14] for slightly compressible and fully compressible two phase flow models that provides up to 25 times speedup. It has been further extended to black-oil model in 3D [15] for testing its accuracy and scalability for more complicated models. Despite computational improvements, the sequential refinement procedure can be viewed as a geometric multigrid method, which commonly suffers from high frequency residuals that originates from the linear interpolation of a coarse solution onto fine unknowns. In response, smoothing algorithms are implemented to remove the high frequency residuals prior to solving the system. For linear problems, [25] introduced an energy minimization method which solves for a coarse basis function that minimizes the energy functional on the fine grid. Li and Wheeler [16] extended such idea to nonlinear problems as local residual minimization by solving a local problem on the refinement domain with boundary conditions provided by linear interpolation of the coarse solution. The local residual minimization mainly removes high frequency residuals caused by saturations while the ones caused by pressure are yet to be resolved. In this section, we will introduce the local coupling formulation to the space-time algorithm for global pressure smoothing. Before that, we will first present some recent improvement on local saturation smoothing for a more stable performance, which in return facilitates global smoothing efficiencies. The results presented below are obtained with slightly compressible flow model.

6.1. Local residual minimization

Previous work [16] has indicated that local residual minimization method is effective in removing high frequency residuals caused by inaccurate saturation initial guess. Such residuals often appear at the channel boundary where the significant contrast in permeability causes the saturation distribution to be discontinuous and the linear interpolation fails to capture such behavior. Here, a local problem is solved by optimization on the refinement domain as follows:

$$\min_{p^n_{\alpha,h},s^n_{\alpha,h}} \left\{ \left\| \int_{E_{i,H}} \left(\partial_t \left(\phi \rho^n_{\alpha,h} s^n_{\alpha,h} \right) + \nabla \cdot \boldsymbol{u}^n_{up,\alpha,h} - q_\alpha \right) w \right\|_\infty \right\} \quad \forall E_{i,H} = \cup_{E_{j,h} \subsetneq E_{i,H}} E_{j,h} \,, \tag{6.1}$$

subject to

$$\begin{cases} p_\alpha = p_{\alpha,\zeta} \\ s_\alpha = s_{\alpha,\zeta} \end{cases} \quad on\ \partial E_{i,H} \,. \tag{6.2}$$

$E_{i,H}$ is any element in the coarse partition $\mathcal{T}^n_H$ being refined into elements $E_{j,h}$ of a finer partition $\mathcal{T}^n_h$. The subscript ζ denotes linear interpolation in space. Although improving the initial guess, the local problem solution process sometimes encounters stability issues due to the inexact boundary conditions. More importantly, the local system cannot establish a definite flow path in subdomains with complex channel structures providing very limited coefficients.

An oversampling technique has been introduced in numerical homogenization algorithms [4,6] for more accurate upscaling of problems with discontinuous coefficients, namely channelized permeability in our case. We apply a similar idea to local residual minimization as demonstrated in Fig. 14. Here, a coarse grid with underlying fine mesh is illustrated. The original local domain $E_{i,H}$ is extended to $E^+_{i,H}$ by oversampling. To solve the local problem on the original domain, a 5 point stencil (left plot: red arrows) is sufficient to interpolate the boundary nodes (right plot: red circles). However, to solve such a problem on the oversampled domain, a 9 point stencil (left plot: red and blue arrows) is required to accurately interpolate the extended boundary nodes (right plot: blue circles).

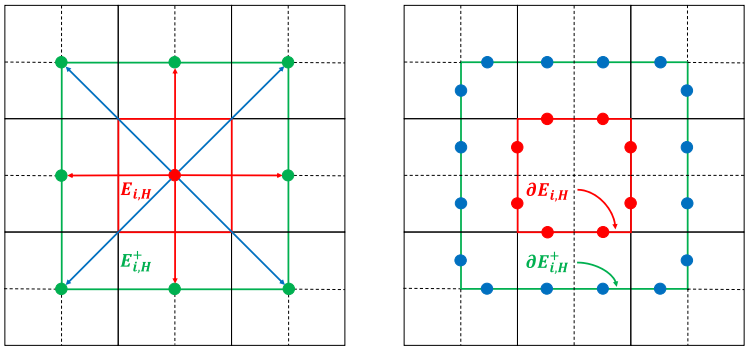

Fig. 14. 5 point stencil (red arrows) and 9 point stencil (all arrows) to interpolate original domain boundary nodes (red circles) and oversampled domain boundary nodes (blue circles).

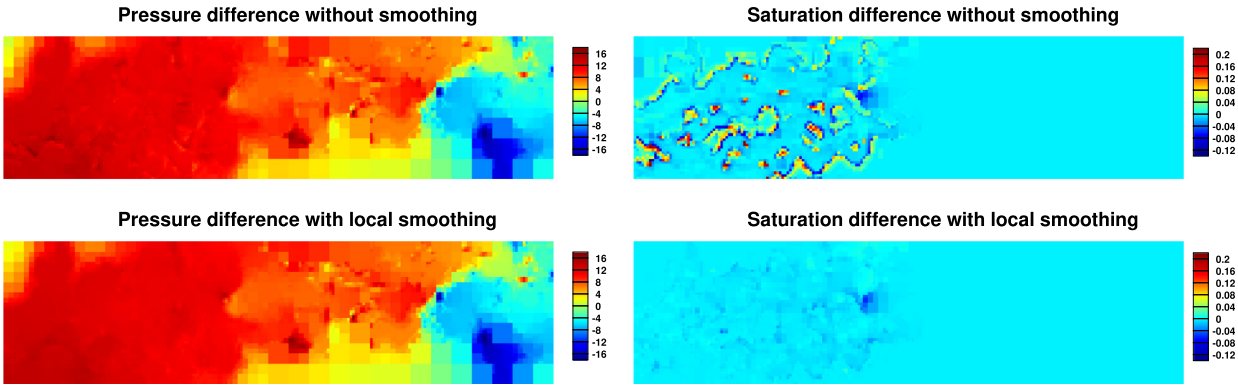

Fig. 15. Pressure and saturation difference between initial guess and converged solution with and without local smoothing.

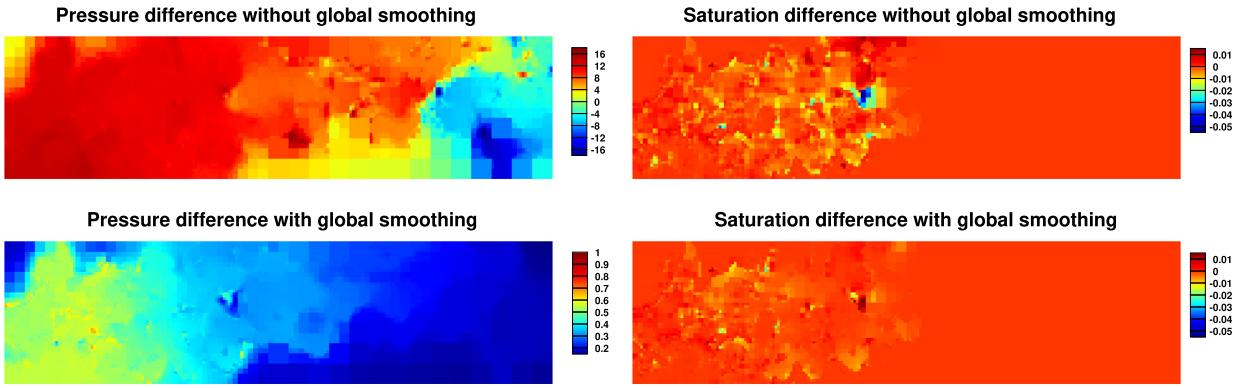

Fig. 16. Pressure and saturation difference between initial guess and converged solution with and without local and global smoothing.

The improvement on the initial guess is illustrated in Fig. 15. We observe significant mismatch between the saturation initial guess and final solution along the channel boundary since the linear interpolation is unable to capture the discontinuous behavior of the solution in such region. Fortunately, after local residual minimization, most of the major discrepancies have been eliminated with some minor ones remaining in the front region. Although improving saturation initial guess, we do not perceive noticeable remediation on pressure mismatch other than removing the oscillations. Therefore, further smoothing is still necessary.

6.2. Global smoothing

Preliminary experiments attempted to reduce the pressure discrepancies by simply solving the pressure system with saturations fixed. While making improvements in the steady state domains, such approach augments the mismatch in the front region and sometimes can cause divergence, since the solution in such domain also depends heavily on the saturations. We

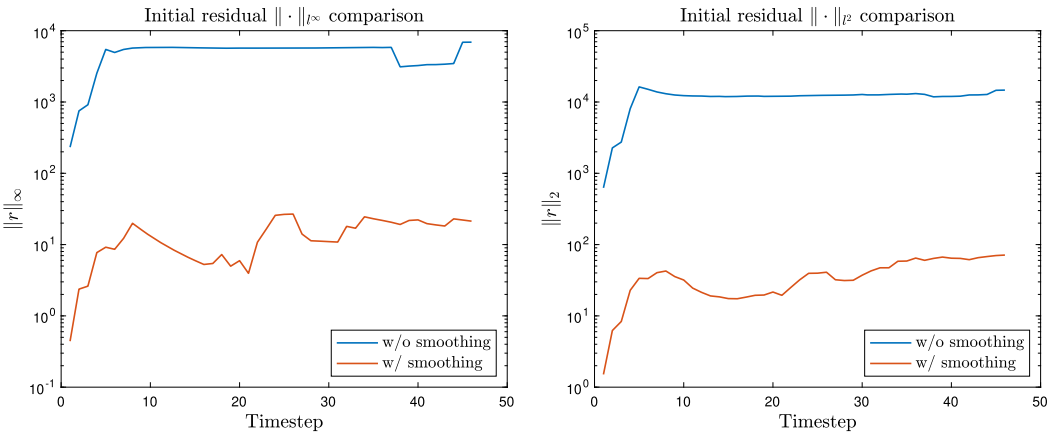

Fig. 17. l_∞ and l_2 norm of initial residual with and without smoothing.

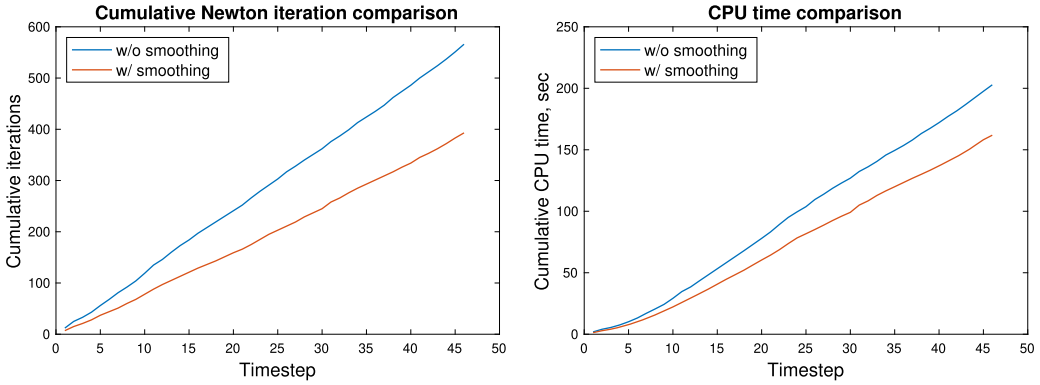

Fig. 18. Cumulative Newton iteration and CPU time comparison for space-time algorithm with and without smoothing.

now use a local coupling approach to provide global pressure smoothing. The space-time algorithm already outlined subdomains with strong transport-diffusion coupling by applying temporal refinements and thus saturation unknowns in the regions with local timesteps are attached to the pressure system. The mismatch in pressure and saturation after global smoothing is plotted in Fig. 16. Note that the color scale for pressure difference after global smoothing is reduced significantly to illustrate the minor discrepancies. We observe that the pressure mismatch have been reduced to under 1 *psi* and the saturation initial guess in the front region is also further enhanced.

We quantify the improvement made on the initial guess using the initial residual before the Newton iterations. The result is presented in Fig. 17. We observe that the maximum and average residual has been reduced by approximately 3 orders of magnitude. With the adequate initial guess, the cumulative nonlinear iterations for the space-time algorithm has been reduced by 40%, as illustrated in Fig. 18. There is also 20% saving on the total CPU time.

7. Conclusions

In this paper, we propose a local coupling strategy with two variant algorithms to solve the advection-diffusion equation in decoupled fashion without causing any increase in nonlinear iterations or divergence issues. The saturation unknowns in the outlined subdomain is coupled with the global pressure system to be solved monolithically. The timestep dynamic method determines a coupling subdomain for each timestep and the region is unchanged during the Newton iterations of the timestep. The iteration dynamic approach on the other hand updates the local coupling domain every iteration. Regions with achieved mass balance are excluded from the main system and the saturations within are no longer updated. We use the proposed algorithms to conduct numerical experiments with slightly compressible and fully compressible fluid models. The results demonstrate that local coupling schemes generally follow the same nonlinear convergence path as the fully implicit method. Therefore, there is no noticeable increase in total iterations to solve the system. The CPU time is reduced by 50% to 75%. However, we do observe a sharper increase in CPU time of the timestep dynamic algorithm during late simulation time for the slightly compressible case due to the growing size of the coupling subdomains. The error of pressure and saturation solution is generally minimal. The error from the iteration dynamic method is larger since the saturation is no longer updated once a region is decoupled. Such effect is more noticeable in the fully compressible model.

These results suggest that combining both decoupling schemes can resolve the sharp increase in CPU time during later time while ensuring solution accuracy. Preliminary experiment attempted such strategy indicates that a more detailed algorithm to update the local coupling subdomain is necessary to avoid unstable nonlinear convergence. We also applied the local coupling concept to the space-time geometric multigrid method as a global pressure smoother. The initial residual after multigrid prolongation is reduced by approximately 3 orders of magnitude and the nonlinear iteration count is decreased by 40%, providing a 20% saving on CPU time. Although originated from advection-diffusion problems, the local coupling strategy provides a possible solution to resolve more complex multi-physics system such as fluid-structure interaction and non-isothermal flow.

CRediT authorship contribution statement

Hanyu Li: Conceptualization, Methodology, Software, Writing – original draft. **Mary F. Wheeler:** Conceptualization, Resources, Supervision, Writing – review & editing.

Declaration of competing interest

The authors declare that they have no known competing financial interests or personal relationships that could have appeared to influence the work reported in this paper.

Data availability

Data will be made available on request.

References

[1] E. Ahusborde, M. Ossmani, A sequential approach for numerical simulation of two-phase multicomponent flow with reactive transport in porous media, Math. Comput. Simul. 137 (July 2017) 71–89.
[2] M. Bause, F. Radu, U. Köcher, Space-time finite element approximation of the Biot poroelasticity system with iterative coupling, Comput. Methods Appl. Mech. Eng. 320 (June 2017) 745–768.
[3] M. Christie, M. Blunt, Tenth SPE comparative solution project: a comparison of upscaling techniques, SPE Reserv. Eval. Eng. 4 (Aug 2001) 308–317.
[4] E. Chung, Y. Efendiev, T. Hou, Adaptive multiscale model reduction with generalized multiscale finite element methods, J. Comput. Phys. 320 (Sept 2016) 69–95.
[5] E. Chung, Y. Efendiev, W. Leung, P. Vabishchevich, Contrast-independent partially explicit time discretization for multiscale flow problems, J. Comput. Phys. 445 (Nov 2021) 110578.
[6] Y. Efendiev, T. Hou, Multiscale Finite Element Methods: Theory and Applications, vol. 4, Springer Science and Business Media, 2009.
[7] B. Fernandes, F. Marcondes, K. Sepehrnoori, A new four-phase adaptive implicit method for compositional reservoir simulation, J. Comput. Phys. 435 (June 2021) 110263.
[8] J. Franc, O. Møyner, H. Tchelepi, Coupling-strength criteria for sequential implicit formulations, in: SPE Symposium on Reservoir Simulation, SPE-203909, Oct 2021.
[9] T. Hughes, G. Hulbert, Space-time finite element methods for elastodynamics: formulations and error estimates, Comput. Methods Appl. Mech. Eng. 66 (Feb 1988) 339–363.
[10] J. Kim, H. Tchelepi, R. Juanes, Stability and convergence of sequential methods for coupled flow and geomechanics: drained and undrained split, Comput. Methods Appl. Mech. Eng. 200 (June 2011) 2094–2116.
[11] J. Kim, H. Tchelepi, R. Juanes, Stability and convergence of sequential methods for coupled flow and geomechanics: fixed-stress and fixed-strain split, Comput. Methods Appl. Mech. Eng. 200 (Mar 2011) 1591–1606.
[12] U. Köcher, M. Bause, Variational space-time methods for the wave equation, J. Sci. Comput. 61 (Nov 2014) 424–453.
[13] D. Krause, R. Krause, Enabling local time stepping in the parallel implicit solution of reaction–diffusion equations via space-time finite elements on shallow tree meshes, Appl. Math. Comput. 277 (Mar 2016) 164–179.
[14] H. Li, W. Leung, M. Wheeler, Sequential local mesh refinement solver with separate temporal and spatial adaptivity for non-linear two-phase flow problems, J. Comput. Phys. 403 (Feb 2020) 109074.
[15] H. Li, M. Wheeler, Implicit space-time domain decomposition approach for solving multiphase miscible flow: accuracy and scalability, SPE J. (SPE-203989-PA) (Sept 2021) 1–12.
[16] H. Li, M. Wheeler, Local residual minimization smoothing for improving convergence behavior of space-time domain decomposition method, in: 26th Domain Decomposition Conference Proceedings, 2021.
[17] J. Li, P. Tomin, H. Tchelepi, Sequential fully implicit Newton method for compositional flow and transport, J. Comput. Phys. 444 (July 2021) 110541.
[18] B. Lu, T. Alshaalan, M. Wheeler, Iteratively coupled reservoir simulation for multiphase flow, in: SPE Annual Technical Conference and Exhibition, SPE-110114-MS, Anaheim, California, Nov 2007.
[19] X. Lu, M. Wheeler, Three-way coupling of multiphase flow and poromechanics in porous media, J. Comput. Phys. 401 (Jan 2020) 109053.
[20] A. Mikelić, M. Wheeler, Convergence of iterative coupling for coupled flow and geomechanics, Comput. Geosci. 17 (July 2013) 455–461.
[21] M. Peszyńska, M. Wheeler, I. Yotov, Mortar upscaling for multiphase flow in porous media, Comput. Geosci. 6 (Mar 2006) 73–100.
[22] G. Thomas, D. Thurnau, Reservoir simulation using and adaptive implicit method, SPE J. 23 (Oct 1983) 759–768.
[23] M. Vohralík, A posteriori error estimates for lowest-order mixed finite element discretizations of convection-diffusion-reaction equations, SIAM J. Numer. Anal. 45 (Aug 2007) 1570–1599.
[24] M. Vohralík, M. Wheeler, A posteriori error estimates, stopping criteria, and adaptivity for two-phase flows, Comput. Geosci. 17 (Oct 2013) 789–812.
[25] W.L. Wan, T.F. Chan, B. Smith, An energy-minimizing interpolation for robust multigrid methods, SIAM J. Sci. Comput. 21 (Dec 1998) 1632–1649.
[26] Z. Wong, F. Kwok, R. Horne, H. Tchelepi, Sequential-implicit Newton method for multiphysics simulation, J. Comput. Phys. 391 (Aug 2019) 155–178.
[27] L. Young, T. Russell, Implementation of an adaptive implicit method, in: SPE Symposium on Reservoir Simulation, SPE-25245-MS, New Orleans, Louisiana, Feb 1993.